Defect-induced exciton localization in bulk gallium nitride from many-body perturbation theory

D. Kirk Lewis and Sahar Sharifzadeh

Understanding defect-induced exciton localization in bulk gallium nitride from many-body perturbation theory

D. Kirk Lewis,[1] Sahar Sharifzadeh[1,2,3]

[1]Department of Electrical and Computer Engineering, Boston University, Boston, MA 02215
[2]Division of Materials Science and Engineering, Boston University, Boston, MA 02215
[3]Department of Physics, Boston University, Boston, MA 02215

Abstract

We present a many-body perturbation theory study of the excitonic properties of wurtzite GaN containing a single charged nitrogen vacancy. We determine that the lowest energy exciton consists of a bulk to defect transition, resulting in a 0.1 eV redshift of the optical absorption onset and a 50 meV increase in the exciton binding energy when compared with pristine bulk. Furthermore, by analysis of the electron-hole correlation function, we quantify the defect-induced localization of the Wannier-Mott exciton in two ways. First, we show that the electron-hole separation is reduced, and that the exciton envelope wavefunction can be related to a simple model of a defect-bound exciton. Second, we show that the exciton center-of-mass does not display the periodicity of the lattice due to defect-induced localization. We anticipate that our approach, which quantitatively describes the influence of a point defect on the exciton wavefunction, will be generally applicable.

Keywords: excitons, point defects, first-principles calculations

1. Introduction

Point defects in semiconductors play an important role in many emerging technologies because they can potentially dominate the properties of optoelectronic materials [1–3]. The localization of electron density near defects can lead to trap states that limit the efficiency of light emitting diodes and transistors [4]. Alternatively, this localization can be utilized to create photocatalytic hotspots [5,6] or to create single photon emitters for use in quantum technologies [7]. Thus, controlling the fundamental electronic structure associated with point defects in materials is of paramount importance. Due to the uncertainty in establishing a relationship between a particular defect and opto-electronic properties from measurements because of the lack of control of the type and density of defects in materials, it is necessary to seek insight from theoretical modeling [8–12].

In particular, the presence of point defects has a significant impact on the absorption and emission spectra of materials. Electron-hole pairs can be trapped at the point defect sites, with their energetics determined by the defect-induced trap states. Additionally, the electron-hole pair can form a bound exciton with strong Coulomb interaction, with further spatial localization and highly efficient recombination [13–18]. In order to understand the nature of the electron-hole pair, it is necessary to characterize both the single particle energy levels and excitonic interactions associated with introduction of the defect. While theory and computation have made great advances in accurately describing trap state energies and recombination rates in defective materials [19–21], there are few computational studies of electron-hole interactions because of the computational complexity associated with capturing this phenomenon. Additionally, there is a lack of quantitative tools to describe the distribution of electron and hole in extended systems (such as exists for finite systems [22–24]), limiting the understanding of exciton localization that can be gained from computation.

Recently, first-principles many-body perturbation theory (MBPT), a method that can accurately capture both electron-electron and electron-hole interactions, has been applied to the study of excitons within defective semiconductors [16,17,25–37]. The optical absorption spectrum from MBPT, computed within the GW and Bethe-Salpeter equation (BSE) approach [38,39] has been shown to provide quantitatively accurate optical absorption energies when compared with measurements [40]. Additionally, MBPT has been especially effective at explaining the detailed mechanisms underpinning measurement by identifying the nature of excited state transitions in defective materials; such calculations have provided the impetus to reexamine commonly accepted interpretations of experimental results in terms of such transitions [15,25].

Here, we present MBPT-based studies of the excitonic properties of bulk wurtzite gallium nitride (GaN) containing a single point defect – the nitrogen vacancy in the +1 charge state (V_N^{1+}) in order to understand defect-induced exciton localization. GaN is a well-studied light emitting material for which there is not always a clear correlation between particular defects and spectroscopic measurements [41,42]. There are also numerous theoretical studies of the energetics of defects in GaN [43,44]. Therefore, it serves as a highly relevant model system with technological applications. We utilize GW/BSE, along with a previously introduced analysis of the electron-hole correlation function [45], to understand the nature and energy of the exciton. Our analysis decomposes the exciton into a center-of-mass and relative envelope correlation function, demonstrating and quantifying the defect-induced localization of the solid-state exciton.

2. Computational Details

The geometry of GaN is taken from Ref. [46]; wurtzite GaN forms a close-packed hexagonal cell with lattice vectors of 3.20 Å along the *a* and *b* axes and 5.20 Å along *c*, in good agreement with measurement [47]. The defect is created by removing a nitrogen atom from a 4x4x3 supercell, which results in a defect-defect separation of 12.8 Å along the *a* and *b* directions and 15.6 Å along *c*.

We compute the optical absorption and excitonic properties of the pristine GaN unit cell and 4 x 4 x 3 defective supercell (Fig. 1) using the BerkeleyGW package [48] with starting DFT orbitals from Quantum Espresso [49] [50]. The DFT and GW calculations follow previous studies [46]; we utilized the local density approximation (LDA) for the DFT simulations with a dielectric function cutoff of 20 Ry. For the pristine bulk unit cell (with-defect supercell) the highest empty state energy used to build the self-energy was 9.1 Ry (5.1 Ry) corresponding to a highest unoccupied state of 146 (3600); for both geometries a previous study [46] showed that GW results for the unit cell were converged at a highest empty state energy of 5.1 Ry corresponding to a highest unoccupied state of 74. For GW calculations a shifted k-point mesh of 8 x 8 x 8 (2 x 2 x 2) was used for the pristine bulk unit cell (with-defect supercell). The BSE sum was expanded over 8 valence x 6 conduction bands for the bulk unit cell and 12 valence x 7 conduction bands for the defective supercell. The k-point mesh used for the BSE sum was 16 x 16 x 16 (8 x 8 x 8) for the unit cell (supercell), with the quasiparticle energies and BSE kernel interpolated from the coarse grid onto the fine grid. For the bulk unit cell, we systematically checked the convergence of predicted BSE eigenvalues and dielectric function with the number of bands and number of k-points. Additionally, we performed GW/BSE calculations on a pristine bulk 4x4x3 supercell with the same convergence parameters as the defective supercell in order to ensure that these computational conditions reproduce the results of the unit cell calculations. We found that the peaks in the dielectric function agree to 0.1 eV. We apply a Gaussian broadening of 0.25 eV to the final BSE spectrum in order to account for the experimental resolution and finite temperature effects.

To account for charged supercell interactions, we apply an average electrostatic correction [51] [52] of 0.1 eV to all defect-centered orbital energies [53] [54] at all k-points of the fine grid. This is important because the localized defect states will be artificially pushed to higher energy due to long-range electrostatic interactions, resulting in an error in their relative energy to the bulk bands. This correction results in ~ 100 meV red shift of the BSE-calculated onset of absorption. In addition, this correction lowers the energy of unoccupied defect states with respect to the bulk CBM, altering the nature of the excited-state.

We analyze the nature of the exciton wavefunction by evaluating the dominant transitions in the BSE sum and evaluating the spatial distribution of the wavefunctions. To evaluate the dominant transitions of the exciton, the orbitals shown in Fig. 1b-c are weighted orbitals, scaled by the coefficients determined by solving the Bethe-Salpeter Equation where the exciton wavefunction is represented as a linear combination of Kohn-Sham orbitals [38]. To make numerical calculations of the electron-hole correlation function of Eq. 2 and center-of-mass (COM) correlation function of Eq. 6, we perform the integral over the hole coordinate as a sum over many hole positions. We choose a series of random hole positions within the unit cell (pristine bulk) or 4 x 4 x 3 supercell (defective bulk), increasing the number of hole positions until significant changes in $\mathcal{F}$ have ceased. We found that using 50 (200) random hole positions were adequate to determine $\mathcal{F}$ for the pristine (with-defect) system. The COM function is a function of the sum of electron and hole coordinates, and is much more sensitive to hole sampling than the ECF, which depends on their difference; to describe the fully periodic COM, it is necessary for hole positions to be sampled beyond a single unit cell. Therefore, we calculated this function sampling hole positions within a 5 x 5 x 5 supercell using 50 randomly placed holes. Additionally, in order to check the

significance of defect-defect interactions on the distribution of $\mathcal{F}_d(\boldsymbol{r})$, we applied a cutoff such that r is contained within a single 4 x 4 x 3 supercell; we determined that defect-defect interactions did not have a notable impact on the extent of or fit to $\mathcal{F}_d(\boldsymbol{r})$.

3. Results
   i. *Defect-induced changes in low-energy optical transitions*

Fig. 1a presents the calculated imaginary part of the dielectric function for both pristine and defective GaN. For the pristine bulk unit cell, we predict an onset of absorption at 3.34 eV, in good agreement with experiment [55]. Moreover, as shown in the figure, the absorption spectrum of pristine bulk agrees well with measurement up to a range of 8.0 eV. As shown in Fig. 1a inset, with the introduction of the defect, the onset of absorption slightly redshifts to 3.3 eV; the small shift suggests that the defect constitutes a small perturbation. Additionally, there is an increase in oscillator strength of the lowest energy peak with introduction of defect, indicating that the electron-hole separation is reduced compared to the bulk. We predict an exciton binding energy, calculated as the energy difference between the free electron-hole pair and the bound exciton, to be 81 meV for the pristine and 126 meV for the with-defect structure. Our finding is consistent with experimental studies of nitrogen vacancies in GaN in which a slight redshift of the photoluminescence onset upon introduction of the defect has been observed [56]. The slight increase in exciton binding is also consistent with a more localized exciton wavefunction.

We note that the pristine GaN exciton binding energy is overestimated with respect to the Bohr model when parameters are taken from measurements (18-28 meV) [57–64] and from previous many-body perturbation theory calculations (30-37 meV) [65,66]. That the calculations overestimate experiment may be due to the fact that we do not account for ionic screening which can be significant in GaN and would lead to reduction in the binding energy. Additionally, there are inherent errors associated with GW/BSE and its input parameters. In particular, previous calculations [65,66]. used a finer k-point grid than we do in the current study.
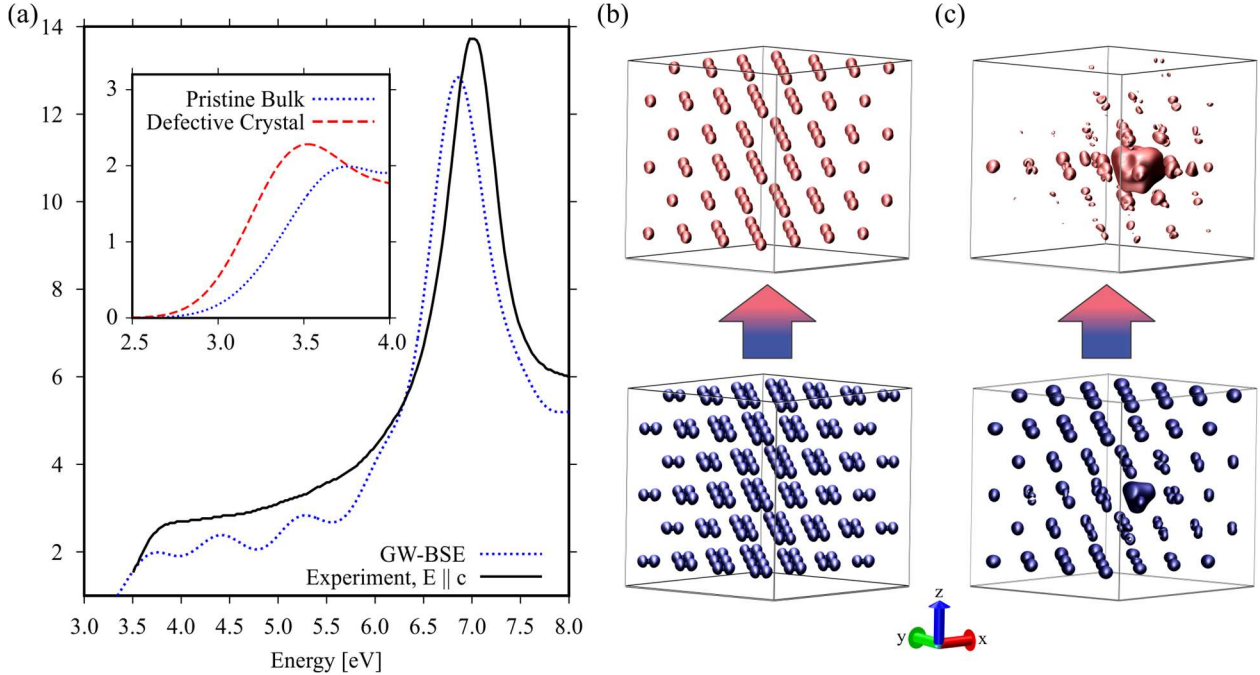

Figure 1. a) The imaginary part of the dielectric function of pristine wurtzite GaN compared with ellipsometry measurement [67]. The inset shows the change in onset of absorption when the V_N^{1+} defect is introduced. The transition associated with the lowest energy exciton is shown for b) pristine bulk and c) with-defect structure. For b-

c, the blue and red density plots show the hole and electron component of the transition, respectively. For all calculations the polarization of the electric field is parallel to the GaN c-axis, consistent with the experiment.

In our previous studies, we found that this defect introduces four defect-centered electronic states into the band structure of GaN, with energies near the bulk band edges [46]. These states include one occupied state deep within the valence band (0.2 eV from the valence band maximum) with spherical *s*-type symmetry and three unoccupied states near the bottom of the conduction band with *p*-type symmetry. Because these states are within the bands, we expect that the exciton will be a combination of bulk-like and defect-like excitations; the dominant transitions associated with the excited-state (Fig. 1b-c) confirm this expectation. For pristine bulk, the lowest energy exciton is a valence band (VB) to conduction band (CB) transition, which is to be expected for this direct gap semiconductor. Here, the VB is mainly composed of nitrogen *p*-type orbitals while the CB is mainly composed of nitrogen *s*-type orbitals. In the presence of the V_N^{1+} defect, the lowest-energy exciton associated with the defective structure consists of a transition from bulk-like VB to a localized defect-centered orbital, with the electron density centered around the defect and distributing over nearest neighbor gallium atoms.

Fig. 1c indicates that the lowest energy exciton state in the presence of the defect is neither a defect-to-defect nor bulk-to-bulk transition, consistent with a weak perturbation to the system. This explains why the onset of absorption and exciton binding energy are only modestly affected by the presence of defect. However, the analysis indicates a delocalized hole and localized electron distribution, which will influence the nature of the exciton.

ii. Defect-induced exciton delocalization

In order to better understand the nature of the exciton in the presence of the defect, we analyze the two-particle (electron-hole) wavefunction in terms of the well-known Wannier-Mott model for an exciton in a periodic solid. Here, the exciton wavefunction is derived from effective mass theory [68] as a product of non-interacting electron and hole wavefunctions (i.e. one-electron orbitals), and an envelope function that localizes the exciton via the Coulomb interaction. For a nearly-free electron system with low carrier effective masses and high screening, the electron and hole will be spatially well separated forming a Wannier-Mott exciton. The periodicity of the crystal results in a Bloch invariant wavefunction that is a function of the center-of-mass coordinate, $r_{cm} = \frac{m_e r_e + m_h r_h}{m_e + m_h}$, while the relative envelope function within the medium is a function of the relative coordinates, $r = r_e - r_h$. The former defines where in the lattice the electron-hole pair resides, while the latter provides a measure of electron-hole binding and localization.

The relative envelope function can be described by a hydrogenic Hamiltonian and the associated lowest energy exciton state is a 1*s*-type orbital with spatial extent defined by the Bohr radius, $a = a_0(\epsilon/\mu)$. Here, a_0 is the hydrogen Bohr radius, $\mu = 1/(1/m_e + 1/m_h)$ is the exciton reduced mass, and ϵ is the dielectric constant. The exciton Bohr radius defines the distance between electron and hole and is highly relevant for determining energetics as well as recombination rates.

The Wannier-Mott model has been shown to work very well in predicting exciton binding energies when compared with experiment for a series of semiconductors [68]. However, the perturbation due to the defect state will qualitatively and quantitatively influence both the envelope and center-of-mass functions. In particular, the crystalline symmetry is broken by presence of the defect, and both electron and hole can be more spatially localized at the defect site. Thus, the envelope function will decrease in size and the center-of-mass function will not be Bloch invariant.

Previously, the localization of excitons near an ionized donor impurity has been described within effective mass theory [69], with the exciton Hamiltonian expressed as

$$H_d = -\frac{\hbar^2 \nabla_e^2}{2m_e^*} - \frac{\hbar^2 \nabla_h^2}{2m_h^*} - \frac{e^2}{\epsilon r_e} + \frac{e^2}{\epsilon r_h} - \frac{e^2}{\epsilon r}. \tag{1}$$

Here, the first two terms define the kinetic energy of non-interacting electron and hole with effective masses of m_e and m_h, respectively, the third and fourth terms define the electron and hole binding to the defect, respectively, and the last term is the electron-hole Coulomb attraction. It has been shown that a trial wavefunction function taking the form of a linear combination of exponentially decaying functions can be fit to experimental data to provide insight into excitonic properties [70]. In the following, we investigate the applicability of the Wannier-Mott model and the model of Ref. [70] to the pristine and defective GaN by analysis of the predicted GW/BSE wavefunction in terms of its center-of-mass and envelope components.

Fig. 2 presents a measure of the envelope function -- the electron distribution when the hole is localized in a high probability location. For pristine GaN, the electron distribution is consistent with a Wannier-Mott type exciton; because of the hexagonal symmetry of the crystal, there is a slight asymmetry to the exciton along the c-axis better described as a Wannier-Mott exciton within an anisotropic medium. For the with-defect structure, the electron density no longer resembles a Wannier-Mott-type exciton: the distribution around the hole is much more localized and highly asymmetric. This more localized electron-hole distribution is consistent with the increased oscillator strength in the first absorption peak and increased exciton binding energy.
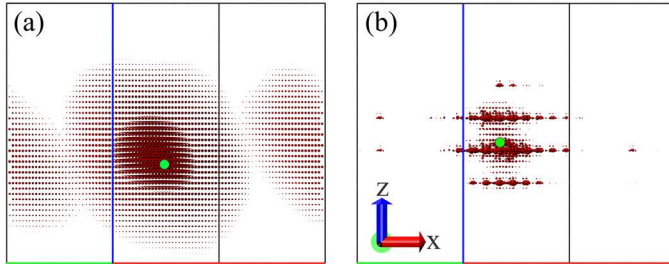

Figure 2. Plot of the electronic density associated with the exciton wavefunction with the hole localized in a high probability location (green circle) for a) pristine GaN and b) with-defect GaN.

In order to quantitatively describe the exciton envelope function in the solid-state, we define the electron-hole correlation function, i.e. the probability of finding electron and hole separated by a vector, $\mathbf{r}$ [45]. This function provides a definition of delocalization lengths, charge transfer character, and asymmetry associated with the exciton wavefunction, and importantly for our defective system where the underlying GaN translation symmetry is broken, does not rely on choosing a specific hole position for describing the exciton wavefunction. Previously, we introduced the envelope electron-hole correlation function (ECF) [27],

$$\mathcal{F}(\mathbf{r}) = \frac{\int |\Psi(r_e = r + r_h, r_h)|^2 d^3 r_h}{\int |\Psi(r_e)\Psi(r_h)|^2 d^3 r_h}, \tag{2}$$

where, $\mathbf{r}_e$ and $\mathbf{r}_h$ define the electron and hole coordinates respectively and the integral is taken over the total volume of the crystal. Here, the numerator is an integral over the volume of the interacting electron-

hole wavefunction[1] and the denominator an integral over the volume of the non-interacting electron and hole obtained from the random phase approximation (RPA) as a simple product of the highest energy valence and lowest energy conduction Kohn–Sham wave functions. $\mathcal{F}(\boldsymbol{r})$ is not the envelope wavefunction but does analogously provide the electron-hole distribution of the exciton (see [71] for relationship).

Given the Wannier-Mott exciton wavefunction, the ECF for lowest energy state, which is expected to be valid for the pristine GaN, takes the form

$$\mathcal{F}_p^{Wannier}(\mathrm{r}) = A_0 e^{-\frac{2r}{a}}, \tag{3}$$

where r is the radial coordinate, A_0 is a normalization constant, and the subscript indicates a pristine defect-free material (see [71] for derivation).

Figs. 3a-b show the calculated $\mathcal{F}_p(\boldsymbol{r})$ along the xy and xz crystallographic planes of pristine GaN, respectively, with the function integrated over the third axis. The function peaks at (0, 0) where electron and hole occupy the same space, and drops off over a ~1 nm radius. The spatial extent of the function is consistent with a Wannier-Mott exciton in an anisotropic medium [72]. The spatial extent is shown in Fig. 3e, which presents the radial distribution of the ECF $\mathcal{F}_p(\mathrm{r} = |\mathbf{r}|)$. Fitting this function to Eq. 3 (Fig. 3e), we find an excellent fit ($R^2 = 0.996$) with decay length (a/2) of 1.13 nm. This corresponds to a Bohr radius of 2.27 nm in reasonable agreement with the anisotropic effective mass model [72], which predicts a Bohr radius of 1.8 nm given average hole and electron effective masses of 1.4 and 0.2, respectively, and dielectric constant of 5.45 for bulk GaN.
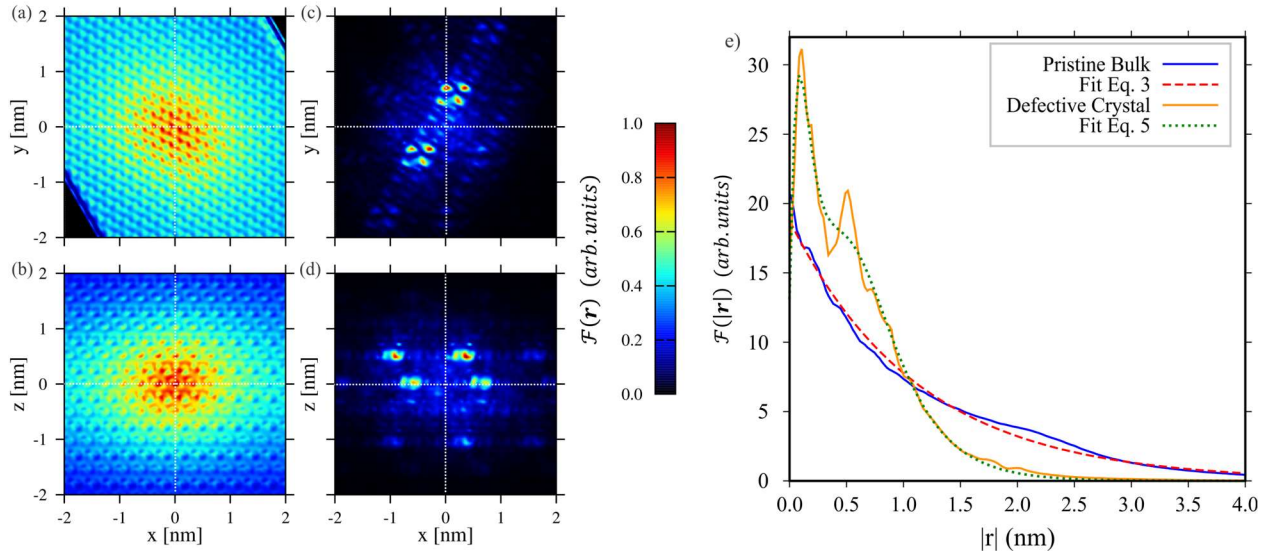

Figure 3. The two-dimensional ECF $\mathcal{F}(\boldsymbol{r})$ for pristine (a,b) and with-defect (c,d) GaN, where $\mathcal{F}(\boldsymbol{r})$ has been averaged over the *c*-axis (a,c) and the b-axis (b,d). The radial ECF, $\mathcal{F}(\mathrm{r} = |\mathbf{r}|)$, for both pristine unit-cell and with-

---

[1] We note that this definition is similar to the definition of electron-electron correlation via the "intracule" approach of e.g. Ref. [74].

defect geometries are shown in e), along with fits to respective models. For the defective structure in e), the two peaks are located at 0.1 and 0.5 nm.

As expected, with the introduction of defect, the Wannier-Mott model is no longer a good fit to the data. Fig. 3c-d present the defective GaN ECF, $\mathcal{F}_d(r)$, in the xy and xz planes, with the function averaged over the c and b crystal planes, respectively. This function is anisotropic in both planes with significant structure. Within the xy plane, the function shows two groupings of peaks centered at electron-hole separation of (0.14, 0.56) nm and (-0.50, -0.53) nm. There are four peaks within these two groupings, located at (0.02, 0.70) nm, (0.35, 0.70) nm, (0.22, 0.47) nm, (-0.10, 0.45) nm, (-0.61, -0.39) nm, (-0.29, -0.40) nm, (-0.40, -0.64) nm, (-0.73, -0.66) nm which all decay on the order of ~ 0.1 nm. Within the xz plane, there are four well-defined separate peaks at locations (0.37, 0.50) nm, (0.73, 0.02) nm, (-0.58, 0.03) nm and (-0.91, 0.50) nm that decay on the order of ~ 0.1 nm. Interestingly, the position of these peaks approximately corresponds to the in-plane nearest-neighbor and multiple next-nearest-neighbor distances. This is consistent with the conclusion of Fig. 1 that the electron is mainly localized near the defect site, extending to the neighboring gallium atoms, while the hole is mainly located in the VB of GaN, which is mainly composed of nitrogen orbitals.

The radial ECF shown in Fig. 3e is also more localized than that that of the pristine GaN. Unlike for pristine bulk, there are multiple peaks in the spectrum, with one prominent peaks at $|r| = 0.1$ nm and a lesser peak at $|r| = 0.5$ nm. The former can be explained as a node in the exciton wavefunction due to the vacancy being in a +1 charge state. The vacancy repels the positive charge and attracts the negative charge, resulting in a node in the electron-hole distribution at $|r| = 0$. The peak at $|r| = 0.5$ nm can be explained by analyzing all of the nearest and multiple next-nearest neighbor distances between gallium atoms adjacent to the defect and nitrogen atoms. Creating a histogram of all distances, we find a peak at 0.47 nm (see [71] Fig. S1). This is again consistent with the nature of the transition shown in Fig. 1c.

With this analysis, we determine that the electron and hole are spatially significantly closer together than in the pristine crystal despite the defect being a small energetic perturbation, and that their relative distribution is highly structure-dependent. Thus, a single hydrogenic function is not suitable for describing the envelope function. Instead, we adapt the trial wavefunction [70] associated with the Hamiltonian of Eq. 1 to a form consistent with our system containing a nearly-free bulk-like hole and trapped localized electron to obtain an exciton wavefunction,

$$\Psi(\mathrm{r} = \mathrm{r}_e - \mathrm{r}_h) = r_h \sum_{i=1}^{N} X_i \, e^{-(A_i r_e + B_i r)}, \tag{4}$$

where the sum runs over N exponential functions with X_i defining the coefficients associated with each term and the B_i defining the decay function of the exponential. This form of wavefunction allows for the structure in the envelope function such as predicted by our GW/BSE calculations. Assuming an ECF of a similar form,

$$\mathcal{F}_d(r) = \left(\sum_{i=1}^{N} X_i \, e^{-B_i r} \right)^2, \tag{5}$$

where, r = |**r**|, we fit the radial ECF of Fig. 3e to this function. Considering four exponential functions, we obtain a good fit of the GW/BSE predicted ECF ($R^2 = 0.97$). Here, the fitted function is able to produce the two main peaks of Fig. 3e with three functions that have decay length of ~ 0.13 nm and one with decay length of ~ 0.7 nm, suggesting that there are multiple length scales associated with the electron-hole wavefunction. Interestingly, the magnitudes of these decay lengths are consistent with the length

scales found in Figure 3. The good fit of the calculated envelope function with this simple model suggests that it can accurately capture the features of the exciton wavefunction.

The prior analysis defines the localization of the electron-hole pair in the relative coordinate. In order to understand the localization of the center-of-mass function with introduction of defect, we calculate the center of mass electron-hole function as

$$\mathcal{F}^{CM}(\boldsymbol{r^{CM}}) = \int \left| \Psi(\boldsymbol{r}_e = \boldsymbol{r^{CM}} - \boldsymbol{r}_h, \boldsymbol{r}_h) \right|^2 d^3\boldsymbol{r}_h. \tag{6}$$

The $\mathcal{F}_p^{CM}$ associated with pristine bulk (see Fig. 4) is delocalized with the periodicity of the unit cell lattice vectors, as is expected for a Wannier-Mott exciton. On the other hand, for the defective structure, $\mathcal{F}_d^{CM}$ is highly localized within the simulated supercell. Thus, the defect not only localizes the electron-hole distribution but also localizes the center of mass of the exciton such that the exciton wavefunction no longer obeys crystal symmetry. Importantly, the center-of-mass localization can be captured by the electron-hole wavefunction analysis introduced in this work.
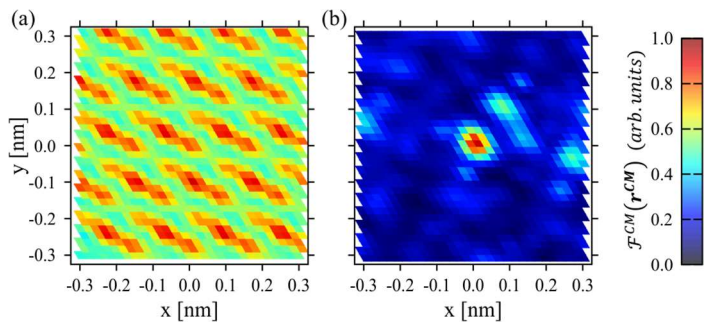

Figure 4. The two-dimensional center-of-mass function $\mathcal{F}^{CM}(\boldsymbol{r^{CM}})$ for (a) pristine and (b) with-defect GaN, where the function has been averaged over the c-axis and normalized to the maximum in the displayed region. In (a), the plot data was shifted to align an arbitrary peak with the plot origin, while in (b) the single dominant peak was shifted to the origin.

4. Conclusion

In summary, we utilized many-body perturbation theory to quantitatively understand the role of a single point defect, V_N^{1+}, on the excitonic properties of GaN. We determined that because the defect introduces states that are resonant with the band energies of the crystal, the exciton energy is only slightly influenced by its presence. However, analysis of the exciton wavefunction reveals that the exciton wavefunction is highly perturbed by the presence of the defect, with a much more localized and anisotropic shape. These features can be captured by a simple model of a trapped electron and nearly-free hole. This study suggests that the defect acts as a perturbation to the Wannier-Mott function – it traps carriers resulting in a more localized exciton, and also induces structural deformations that create a highly anisotropic exciton distribution. We anticipate that the understanding and analytical approach developed here will enable the quantitative description of the excitonic properties of other defective materials.

5. Acknowledgements

[1]   A. H. Wilson, Proc. R. Soc. London A Math. Phys. Eng. Sci. **134**, 277 (1931).

[2]   S. T. Pantelides, Rev. Mod. Phys. **50**, 797 (1978).

[3]   G. A. Baraff, Philos. Trans. R. Soc. London A Math. Phys. Eng. Sci. **341**, 195 (1992).

[4]   E. G. Seebauer and M. C. Kratzer, *Charged Semiconductor Defects: Structure, Thermodynamics and Diffusion* (Springer-Verlag, London, 2009).

[5]   Z. Lin, B. R. Carvalho, E. Kahn, R. Lv, R. Rao, H. Terrones, M. A. Pimenta, and M. Terrones, 2D Mater. **3**, 022002 (2016).

[6]   X. Chang, T. Wang, J. Gong, X. Chang, T. Wang, and J. Gong, in *Semicond. Semimetals* (2017), pp. 429–467.

[7]   I. Aharonovich, D. Englund, and M. Toth, Nat. Photonics **10**, (2016).

[8]   C. Freysoldt, B. Grabowski, T. Hickel, J. Neugebauer, G. Kresse, A. Janotti, and C. G. Van De Walle, Rev. Mod. Phys. **86**, 253 (2014).

[9]   S. Sasaki, K. Kawahara, G. Feng, G. Alfieri, and T. Kimoto, J. Appl. Phys. **109**, 013705 (2011).

[10] N. Iwamoto and B. G. Svensson, in *Defects Semicond.*, 1st ed. (Academic Press, 2015), pp. 369–407.

[11] D. C. Look, Phys. Status Solidi B Basic Res. **228**, 293 (2001).

[12] P. A. Schultz and A. H. Edwards, Nucl. Instruments Methods Phys. Res. B **327**, 2 (2014).

[13] V. L. Bonch-Bruevich and E. G. Landsberg, Phys. Status Solidi **29**, 9 (1968).

[14] U. Schröder, in *Festkoeorper Probl. XIII Adv. Solid State Phys.* (Pergamon, Braunschweig, 1973).

[15] M. Bockstedte, A. Marini, O. Pankratov, and A. Rubio, Phys. Rev. Lett. **105**, 026401 (2010).

[16] S. Refaely-Abramson, D. Y. Qiu, S. G. Louie, and J. B. Neaton, Phys. Rev. Lett. **121**, (2018).

[17] Y. Ma and M. Rohlfing, Phys. Rev. B - Condens. Matter Mater. Phys. **77**, (2008).

[18] S. Ismail-Beigi and S. G. Louie, Phys. Rev. Lett. **95**, 5 (2005).

[19] A. Alkauskas, Q. Yan, and C. G. Van de Walle, Phys. Rev. B **90**, 075202 (2014).

[20] F. Oba and Y. Kumagai, Appl. Phys. Express **11**, (2018).

[21] L. Yu and A. Zunger, Phys. Rev. Lett. **108**, 068701 (2012).

[22] L. Romaner, G. Heimel, H. Wiesenhofer, P. Scandiucci De Freitas, U. Scherf, J. L. Brédas, E. Zojer, and E. J. W. List, Chem. Mater. **16**, (2004).

[23] S. Tretiak, K. Igumenshchev, and V. Chernyak, Phys. Rev. B - Condens. Matter Mater. Phys. **71**, (2005).

[24] F. Plasser, M. Wormit, and A. Dreuw, J. Chem. Phys. **141**, (2014).

[25] P. Rinke, A. Schleife, E. Kioupakis, A. Janotti, C. Rödl, F. Bechstedt, M. Scheffler, and C. G. Van

De Walle, Phys. Rev. Lett. **108**, (2012).

[26]   Y. Ma, M. Rohlfing, and A. Gali, Phys. Rev. B - Condens. Matter Mater. Phys. **81**, (2010).

[27]   M. P. Surh, B. Iiorizonte, and S. G. Louie, Phys. Rev. B **51**, (1995).

[28]   C. Attaccalite, M. Bockstedte, A. Marini, A. Rubio, and L. Wirtz, Phys. Rev. B - Condens. Matter Mater. Phys. **83**, (2011).

[29]   M. L. Tiago and J. R. Chelikowsky, Phys. Rev. B - Condens. Matter Mater. Phys. **73**, 205334 (2006).

[30]   S. Choi, M. Jain, and S. G. Louie, Phys. Rev. B **86**, 041202 (2012).

[31]   M. Bockstedte, A. Marini, O. Pankratov, and A. Rubio, Phys. Rev. Lett. **105**, 026401 (2010).

[32]   M. A. Flores, Semicond. Sci. Technol. **33**, (2018).

[33]   S. Jiang, T. Lu, Y. Long, and J. Chen, J. Appl. Phys. **111**, (2012).

[34]   C. E. Ekuma, J. Phys. Chem. Lett. **9**, (2018).

[35]   C. E. Ekuma and D. Gunlycke, Phys. Rev. B **97**, (2018).

[36]   N. Richard, L. Martin-Samos, S. Girard, A. Ruini, A. Boukenter, Y. Ouerdane, and J. P. Meunier, J. Phys. Condens. Matter **25**, (2013).

[37]   J. Jiang, R. Pachter, and S. Mou, Phys. Rev. B **10**, (2018).

[38]   M. Rohlfing and S. G. Louie, Phys. Rev. B **62**, 4927 (2000).

[39]   G. Onida, L. Reining, and A. Rubio, Rev. Mod. Phys. **74**, (2002).

[40]   X. Leng, F. Jin, M. Wei, and Y. Ma, Wiley Interdiscip. Rev. Comput. Mol. Sci. **6**, 532 (2016).

[41]   M. a. Reshchikov and H. Morkoc, J. Appl. Phys. **97**, 061301 (2005).

[42]   B. Pajot and B. Clerjaud, *Optical Absorption of Impurities and Defects in Semiconducting Crystals* (Springer Berlin Heidelberg, Berlin, Heidelberg, 2013).

[43]   M. Matsubara and E. Bellotti, J. Appl. Phys. **121**, 195701 (2017).

[44]   C. G. Van de Walle and J. Neugebauer, J. Appl. Phys. **95**, 3851 (2004).

[45]   S. Sharifzadeh, P. Darancet, L. Kronik, and J. B. Neaton, J. Phys. Chem. Lett. **4**, 2197 (2013).

[46]   D. K. Lewis, M. Matsubara, E. Bellotti, and S. Sharifzadeh, Phys. Rev. B **96**, (2017).

[47]   O. Lagerstedt and B. Monemar, Phys. Rev. B **19**, (1979).

[48]   J. Deslippe, G. Samsonidze, D. A. Strubbe, M. Jain, M. L. Cohen, and S. G. Louie, Comput. Phys. Commun. **183**, 1269 (2012).

[49]   P. Giannozzi, S. Baroni, N. Bonini, M. Calandra, R. Car, C. Cavazzoni, D. Ceresoli, G. L. Chiarotti, M. Cococcioni, I. Dabo, A. Dal Corso, S. de Gironcoli, S. Fabris, G. Fratesi, R. Gebauer, U. Gerstmann, C. Gougoussis, A. Kokalj, M. Lazzeri, L. Martin-Samos, N. Marzari, F. Mauri, R. Mazzarello, S. Paolini, A. Pasquarello, L. Paulatto, C. Sbraccia, S. Scandolo, G. Sclauzero, A. P. Seitsonen, A. Smogunov, P. Umari, and R. M. Wentzcovitch, J. Physics. Condens. Matter **21**, 395502 (2009).

[50]   J. Enkovaara, C. Rostgaard, and J. J. Mortensen, J. Phys. Condens. Matter **29**, (2017).

[51]   C. Freysoldt, J. Neugebauer, and C. G. Van de Walle, Phys. Rev. Lett. **102**, 016402 (2009).

[52]   C. Freysoldt, J. Neugebauer, and C. G. Van de Walle, Phys. Status Solidi B **248**, 1067 (2011).

[53]   W. Chen and A. Pasquarello, Phys. Rev. B **88**, 115104 (2013).

[54]   M. Jain, J. R. Chelikowsky, and S. G. Louie, Phys. Rev. Lett. **107**, 216803 (2011).

[55]   G. Yu, G. Wang, H. Ishikawa, M. Umeno, T. Soga, T. Egawa, J. Watanabe, and T. Jimbo, Appl. Phys. Lett. **70**, 3209 (1997).

[56]   D. C. Look, G. C. Farlow, P. J. Drevinsky, D. F. Bliss, and J. R. Sizelove, Appl. Phys. Lett. **83**, 3525 (2003).

[57]   J. Y. Duboz, F. Binet, E. Rosencher, F. Scholz, and V. Härle, Mater. Sci. Eng. B **43**, (1997).

[58]   D. G. Chtchekine, Z. C. Feng, S. J. Chua, and G. D. Gilliland, Phys. Rev. B - Condens. Matter Mater. Phys. **63**, (2001).

[59]   A. K. Viswanath and J. I. Lee, Phys. Rev. B - Condens. Matter Mater. Phys. **58**, (1998).

[60]   G. D. Chen, M. Smith, J. Y. Lin, H. X. Jiang, S. H. Wei, M. Asif Khan, and C. J. Sun, Appl. Phys. Lett. **68**, (1996).

[61]   Z. Liu, S. Pau, K. Syassen, J. Kuhl, W. Kim, and H. Morkoç, Phys. Rev. B - Condens. Matter Mater. Phys. **58**, (1998).

[62]   S. J. Xu, W. Liu, and M. F. Li, Appl. Phys. Lett. **81**, (2002).

[63]   M. Steube, K. Reimann, D. Fröhlich, and S. J. Clarke, Appl. Phys. Lett. **71**, (1997).

[64]   J. F. Muth, J. H. Lee, I. K. Shmagin, R. M. Kolbas, H. C. Casey, B. P. Keller, U. K. Mishra, and S. P. DenBaars, Appl. Phys. Lett. **71**, (1997).

[65]   R. Laskowski, N. E. Christensen, G. Santi, and C. Ambrosch-Draxl, Phys. Rev. B - Condens. Matter Mater. Phys. **72**, 1 (2005).

[66]   M. Dvorak, S. H. Wei, and Z. Wu, Phys. Rev. Lett. **110**, (2013).

[67]   C. Cobet, R. Goldhahn, W. Richter, and N. Esser, Phys. Status Solidi Basic Res. **246**, 1440 (2009).

[68]   P. Y. Yu and M. Cardona, *Fundamentals of Semiconductors* (Springer-Verlag, Berlin Heidelberg, 2010).

[69]   P. J. Dean and D. C. Hebert, in *Excitons*, edited by K. Cho (Springer, Berlin, 1979), pp. 55–182.

[70]   T. Skettrup, M. Suffczynski, and W. Gorzkowski, Phys. Rev. B **4**, 512 (1971).

[71]   See Supplemental Material at [URL will be inserted by publisher] for derivation of envelope electron-hole correlation function (ECF) for pristine material, analysis of relationship between physical structure and exciton wavefunction, broadening of calculated absorption data, and effect of averaging on the ECF.

[72]   T. Hanada, in *Oxide Nitride Semicond.*, edited by T. Yao and S. K. Hong (Springer Berlin Heidelberg, 2009), pp. 1–19.

[73]   J. Towns, T. Cockerill, M. Dahan, I. Foster, K. Gaither, A. Grimshaw, V. Hazlewood, S. Lathrop, D. Lifka, G. Peterson, R. Roskies, J. R. Scott, and N. Wilkins-Diehr, Comput. Sci. Eng. **16**, 62 (2014).

[74]   A. Thakkar, A. N. Tripathi, and V. H. Smith, Int. J. Quantum Chem. **XXVI**, 157 (1984).